JOURNAL OF MATERIALS SCIENCE **33** (1998) 5653–5659

A technique for measuring the 3-dimensional to 2-dimensional conductivity change of YBCO superconductors at the normal-to-superconducting phase change

L. V. HMURCIK
Science and Engineering, University of Bridgeport, Bridgeport, CT 06601, USA APS #MHM741373
E-mail: hmurcik@cse.bridgeport.edu

A. BIDARIAN, B. IBARRA, L. D. MATTHEWS
Physics Department, Southern Connecticut State University, 501 Crescent Street, New Haven, CT 06515, USA

It is well known that conduction in $YBa_2Cu_3O_7$ (YBCO) is by means of copper "planes" and "chains," where planes and chains describe the degree of bonding between copper and oxygen. Changes of conductivity versus temperature have been used to show that conduction in YBCO in the normal state is 3-dimensional, while conduction approaching the onset of the superconducting state is first 2-dimensional and then 3-dimensional. We have found another method to monitor this 2-to-3 transition. Using square samples, and measuring the voltage at each corner caused by a current applied to the opposite corners, one can find the conductivities along the x-axis and the y-axis. The ratio of these conductivities is unity for homogeneous samples in the normal state. However, in transition to the superconducting state, the ratio of conductivities changes. We examine this change as a function of sample purity, sample history, and exposure to an external magnetic field. Our data are consistent with data reported in the literature, and they suggest the existence of another state change deep in the superconducting state, which is only observable with the application of a magnetic field.

Measurements were also carried out to correlate the anisotropy with sample porosity. Measurements of normal state resistivity, critical temperature, and critical current characterize the sample's porosity, and these data affect the anisotropy in the superconducting state in a manner directly proportional to the porosity.

1. Introduction

The superconductor $YBa_2Cu_3O_7$ (YBCO) has been extensively studied. Two concepts have been the focus of attention in the present literature. The first deals with the mode of conduction above the critical temperature (T_c). From room temperature to ($T_c + x$) (where x is between 10 and 50), YBCO is metallic in behavior, and its normal-state conductivity obeys either of two equations:

$$\rho = A/T + BT \tag{1}$$

$$\rho = A + BT \tag{2}$$

Some authors [1, 2] report their data to fit the first equation, while others' data fit the second [3–5]. Furthermore, even when data are fit to Equation 2, they can also be fit to Equation 1, but the correlation is much poorer [4, 5]. The reason for this difference is thought to lie in the material's anisotropy. Perfectly crystalline samples (i.e., de-twinned single crystals) exhibit strong anisotropic behavior. If we define the principal planar axes as a and b, and if we define the out-of-plane axis as c, then $\rho_a = \rho_{(CuO2\ plane)}$ and $\rho_{(Cu-O\ chain)} = \rho_a\rho_b/(\rho_a - \rho_b)$, and $\rho_a = A + BT$ (with A almost zero, i.e., no zero-temperature residual resistivity) and $\rho_b = A + BT^2$ [6–9]. The T^2 dependence of ρ_b indicates phonon scattering, while the linear dependence of T is strongly metallic. The variation of ρ_c with temperature is not completely clear, except that it exhibits an insulating behavior and is inversely dependent on temperature (i.e., it goes down as T goes up); it obeys an equation of the form [10, 11]

$$\rho_c = A/T + BT + C \tag{3}$$

Our samples are homogeneous and polycrystalline. Because $\rho_c \gg \rho_b > \rho_a$, they strongly obey Equation 2

above $(T_c + X)$, where X is approximately 20 for our samples; their behavior is metallic. Below $(T_c + X)$, the conduction process changes. If we define the normal resistivity (ρ_N) to be the high-temperature resistivity (given by Equation 2), then the total resistivity is

$$1/\rho = 1/\rho_N + \Delta\sigma \tag{4}$$

where $\Delta\sigma$ is called the excess conductivity, the fluctuation conductivity, or (more commonly) the paraconductivity [5, 12–14]. The paraconductivity varies with temperature as

$$\Delta\sigma \sim \varepsilon^{-\nu} \tag{5}$$

where $\varepsilon = (T - T_c)/T_c$, $\nu = (2 - d/2)$, and d is the sample's fractal dimension, which represents the behavior of the conduction process. Note that $\nu = 1, 1/2$ when $d = 2, 3$. For YBCO, the paraconductivity occurs in two stages. When the temperature is less than about $(T_c + 20)$ but greater than about $(T_c + 5)$, the superconduction process starts to occur as CuO_2 planes begin to conduct. Because the conduction is mainly a planar process at this point, $d = 2$. When the temperature drops below approximately $(T_c + 5)$ but is still above T_c, the Cu–O chains participate in the conduction process, as well. The conduction is fully 3-dimensional, and $d = 3$. The temperature ranges over which these different types of conduction occur are not exact. They are mainly a function of the oxygen defect of the superconductor. If the stoichiometric value of the oxygen in the YBCO sample is n (with $6 < n < 7$), then for $n = 6$ we have a perfect insulator, and for $n = 7$ the Cu–O chains act as electron reservoirs for charge transfer between CuO_2 planes [7, 8]. As n decreases from 7, the interplane distance increases and the conductivity of the chains decreases due to oxygen defect states [13, 15].

As the temperature drops below T_c, YBCO is fully superconducting (although this is impaired by the application of a magnetic field, as we discuss later). In this temperature regimen, the theories and reported data about 2- and 3-dimensional conduction as well as sample anisotropy are virtually non-existent. It is difficult enough to characterize the sample's anisotropy above T_c, where the data are comparatively large and stable. Below T_c, resistivity is greatly diminished, and specific components of resistivity are even harder to isolate. We have been able to duplicate the results summarized in Equations 2, 4, and 5 with $d = 2,\ 3$ as $T \to T_c$. Also, we extended our study to anisotropy and dimensionality studies well below T_c. We use the four-probe method of van der Pauw [16] to measure resistivity. Our samples are $13.5 \times 13.5 \times 1.5$ mm polycrystalline pellets. With the sample lying flat in the xy-plane, we abrade a rounded groove (1/2 mm radius) into each corner where we apply a silver contact. If we number our corner contacts 1, 2, 3, 4, then a complete van der Pauw measurement requires finding voltage across contacts 1, 2 when current flows through 3, 4 and finding voltage 2, 3 for current 1, 4. However, using this data (and no other new data) one can characterize the sample anisotropy in the xy-plane [17–19]. After finding ρ using the standard van der Pauw equation, this can be related to values of ρ_x and ρ_y as [20]

$$\rho^2 = \rho_x \rho_y \tag{6}$$

If we define the anisotropy factor, K, as:

$$K = \rho_y/\rho_x$$

then for a perfect isotropic material $K = 1$. When the two resistivities are not equal, K can be greater or less than 1. (See the Appendix.)

[17] and [18] assume that the contacts to the sample are points in each of the corners of the top square face. The equations they develop to calculate K are extremely lengthy and cumbersome to implement. Furthermore, because the contacts are not points in reality but do have a non-zero dimension, their equations are slightly inaccurate. [19] and [20] assume the contacts are lines along the sample corner edges. The equations are far easier to implement. But even if these "lines" take on a non-zero dimension and become quarter-cylinders (as in our case), the equations do not change. Furthermore, the equations used in [17] and [18] give the same results as [19] and [20] if the sample length and width are ten times the sample thickness [21]. For these reasons, we used the method of [19] and [20] to calculate K.

2. Experimental results and discussion

Samples of polycrystalline YBCO samples were prepared in the usual manner [22–24]. Using Y_2O_3, $BaCO_3$, and CuO as starting materials, a 1 : 2 : 3 composition was calcined at 900 °C for 12 h in air. The powder was ground and pressed into square pellets 13.5 mm on edge. The thickness was dependent on the stamping pressure but was nominally 1.5 mm. The pellets were then treated at 940 °C for 12 h in air. Samples were abraded at each corner, and electrical contacts were added, as previously discussed. All of our samples were prepared to be chemically identical and were only distinguished by the pressure used to stamp them into pellets. Table I lists some of the samples used in this study. They were chosen to cover the range of stamping pressures used.

It was expected that the different stamping pressures would affect sample porosity, and this, in turn, would affect the critical temperature, the resistivity, and the anisotropy [25–28]. As a first-order approximation, assume that the normal state resistivity varies directly with porosity [25]. Consider the normal state resistivity of all samples at $T = 130$ K. (Other temperatures above 130 K were also chosen, and this analysis repeated; the results were similar.) Using a least-squares fit, the normal state resistivity varies with stamping pressure P as

$$\rho = 2.18 \times 10^{-3} \exp(0.0223P) \tag{7}$$

for stamping pressures between 8 and 40 kPSI, and

$$\rho = 3420\ P^{-3.42} \tag{8}$$

TABLE I A list of parameters for five selected samples of polycrystalline YBCO versus stamping pressure that include normal state resistivity parameters A and B, critical temperature, critical current density, and pinning potential

Sample name	P [kPSI]	A (10^{-3})	B (10^{-6})	T_c [K]	J_c [A/cm^2]	U [meV]
Br8	8	1.91	5.15	91.0	59.4 ± 8.5	16.0 ± 0.6
Br24	24	2.64	7.49	88.9	59.4 ± 7.6	15.3 ± 1.1
Br40	40	5.23	0.36	83.9	25.5 ± 2.6	8.7 ± 0.3
Br60	60	1.11	15.41	87.8	26.3 ± 3.4	25.4 ± 5.0
Br72	72	0.84	5.96	90.1	32.3 ± 5.1	33.1 ± 1.1

for P between 40 and 72 kPSI. In Equations 7 and 8, resistivity is in units of [ohm–cm] while pressure is in kPSI. Data showing the variation of T_c with pressure for five samples are listed in Table I. These data (along with Equations 7 and 8) are consistent with a "hard sphere" model to approximate YBCO grains and their size relative to stamping pressure. Starting with large grains at 8 kPSI, the grain size decreases with increasing stamping pressure as grains are broken down into smaller grains; however, the porosity (the percentage of voids between grains) stays constant or changes very little. The resistivity is dependent on tunneling between grains and is thus exponential in behavior [29]. Above 40 kPSI, the grains remain small but fixed in size. Increasing P improves the bonding between grains, and hence the tunneling. However, the larger effect is the decrease in voids (porosity), which will decrease the resistivity according to a power law [30]. In a similar fashion, T_c increases with decreasing porosity [31].

Fig. 1 shows plots of resistivity versus temperature for five samples chosen to span the range of stamping pressures. Their parameters are listed in Table I. In Fig. 1a, no magnetic field is applied, while in Fig. 1b, a field of 2500 Gauss is used. Data plotted in these graphs were taken at a constant test current of 65 mA. For other test currents between 5 and 95 mA, this data did not change in the normal state. Also, it did not change in the paraconducting/superconducting state for

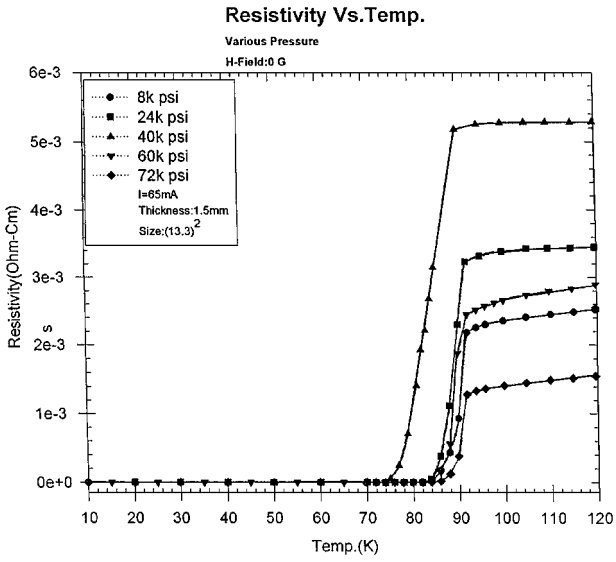

Figure 1a Plots of resistivity versus temperature for five of our polycrystalline YBCO samples at various stamping pressures show a linear dependence of the normal state and a sharp drop in the transition to superconduction. Data up to room temperature (not shown) confirms the linearity of the normal state. See Table I for parameters A and B.

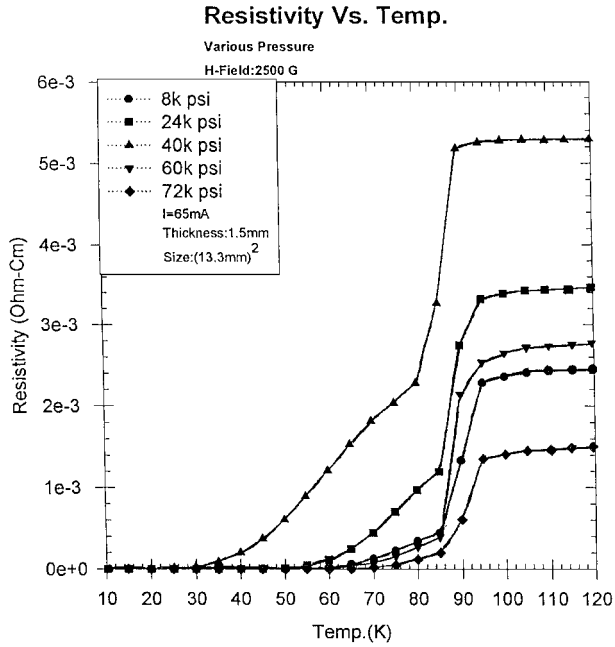

Figure 1b Plots of resistivity versus temperature and stamping pressure with an applied magnetic field (H). The width of the transition region to the superconducting state fits a stretched exponential model.

Fig. 1a. However, there was a major change noted in Fig. 1b for the paraconducting/superconducting state. In simple terms, the transition region between normal and superconducting states widened with the increase in current at a fixed magnetic field perpendicular to the sample face. The data in the transition region of 1B "stretches out" [3, 13, 31] and fits a "stretched" exponential model, where

$$(\rho/\rho_0) = \exp[(-U/kT)((I_c/I)^n - 1)] \qquad (9)$$

and the pinning potential U, the critical current I_c, and n are all functions of the magnetic field. We varied the magnetic field over the range 1000 to 5000 Gauss and found only small changes in our plot of ρ versus T, as expected [3, 13, 31]. With the magnetic field at 2500 Gauss, we varied the current between 5 and 95 mA and recorded large changes in the width of the transition region. Using all of our ρ versus T versus I data, we did a least-squares fit of Equation 9 to find $n = 0.499 \pm 0.035$, which agrees with the value of 0.5 found previously [3]. Our data fit also gave us values of U and I_c and (using information about sample geometry) J_c (the critical current density). See Table I. Critical currents drop as the size of the grain decreases until $P = 40$ kPSI, and then currents stabilize and grow

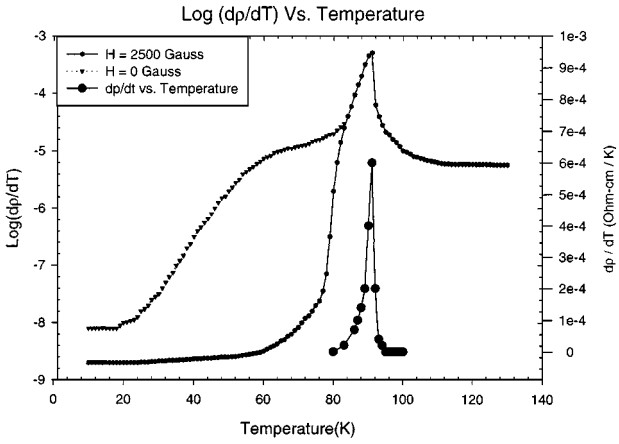

Figure 2 Plots of $d\rho/dT$ and $\log(d\rho/dT)$ clearly show the critical temperature T_c for sample BR8. In addition, the log plot shows a state change below the critical temperature for the application of an external magnetic field.

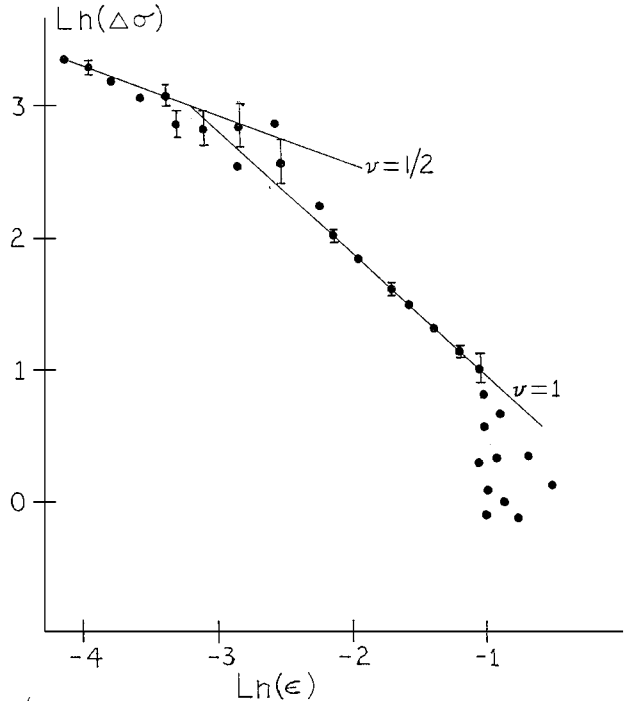

Figure 3 Plot of the paraconductivity versus the reduced temperature ($\varepsilon = (T - T_c)/T_c$) shows that above 119.7 K the normal-state resistivity dominates, between 119.7 and 94.8 K the conduction is 2-dimensional (copper planes), and between 94.8 and 91.0 K the conduction is 3-dimensional (planes and chains).

slowly as grain size changes very little. Pinning potential, on the other hand, first decreases and then increases, because it is most strongly affected by the increase in contact area between grains.

At this point, we should point out how we found the critical temperature. There are several methods listed in the literature [5]:

1. T_c is the midpoint of the transition region between the resistivity's normal and superconducting states.
2. T_c is the intersection on the temperature axis of a straight line formed using the ρ versus T data in the transition region.
3. T_c is the temperature at the onset of superconduction.
4. T_c is the temperature where $d\rho/dT$ is a maximum.

Because the transition region can vary greatly with applied magnetic field and injected current, we found Technique 4 to be the most reliable. Furthermore, we modified this technique so that we plot log $(d\rho/dT)$ versus T. See Fig. 2 for the results of sample BR8. A major change in the width of the transition region caused by the application of the magnetic field does not obscure the location of T_c. Furthermore, we observe a state change in the superconducting region, and this change is not visible in the plot of $d\rho/dT$.

Using the resistivity data for BR8 shown in Fig. 1 (plus other data taken at many different test currents), we can extract the sample paraconductivity. This is done using Equations 4 and 5, and the results are plotted in Fig. 3. (Note that each single data point in Fig. 3 is actually an average determined by 50 separate data points, with 30 of these points measured at different test currents between 5 and 95 mA, and the other 20 accounted for by the variation of the magnetic field. Error bars are shown.) For $92.5 < T < 94.8$ K, the data fit Equation 5 with $\nu = 1/2$, and the conduction process is 3-dimensional, i.e. it is carried out by both copper "planes" and "chains." For $94.8 < T < 119.7$ K, $\nu = 1$, and the conduction is 2-dimensional; copper "planes" are the chief conductors. The data above 119.7 K is too scattered and is considered part of the normal-state region. Thus, the paraconductive state spans a region from $T_c = 91$ K to 119.7 K. Data for the other samples in our study were plotted in a manner similar to Fig. 3. No significant trend could be detected, but in general for all samples:

$$\text{I. } \nu = 1/2, \text{ if } T_c < T < (T_c + x), \text{ and } 2 < x < 7$$

$$\text{II. } \nu = 1, \text{ if } (T_c + x) < T < (T_c + y), \text{ and } 15 < y < 25$$

The results of measuring the YBCO paraconductivity are clear. There is a 2- to 3-dimensional transition in the conduction process when the temperature changes. Furthermore, these results do not change whether there is a magnetic field applied to the sample. The application of the magnetic field (as shown in Fig. 1) increases the effects of grain-boundary scattering and "stretches" the transition region. Hence, the data in Fig. 3 are not affected by grain-boundary scattering but only by transitions within each grain.

Another way to measure the 2- to 3-dimensional transition is by using the modified van der Pauw's equation to find K. Fig. 4 shows plots of K versus T for sample BR8 with no magnetic field applied Fig. 4a and with a 2500 Gauss field (Fig. 4b). With no field, $K = 1$, except in the region where paraconductivity is strongest (from $T_c = 91$ to about 120 K). This coincides with the range of paraconductivity mapped in Fig. 3. For a perfect isotropic conductor, $K = 1$. Therefore, as the temperature drops below 120 K, the anisotropy of each grain undergoing a transition to 2-dimensional copper plane conduction causes K to deviate from unity. The strength of the deviation of K from unity is important

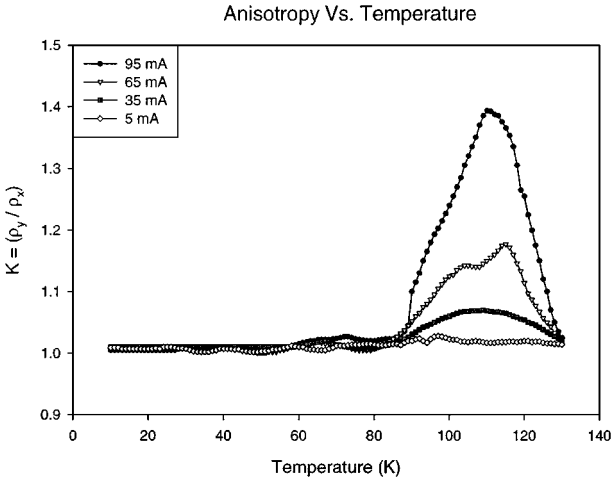

Figure 4a Plots of the van der Pauw anisotropy factor K versus temperature show the sample to be isotropic at all temperatures except in the paraconductive region. Grain-boundary dominance is apparent as a low test current (5 mA) causes almost no significant deviation of K from unity while a strong test current (95 mA) produces a deviation of 38%, i.e., $K_{\max} = 1.38$.

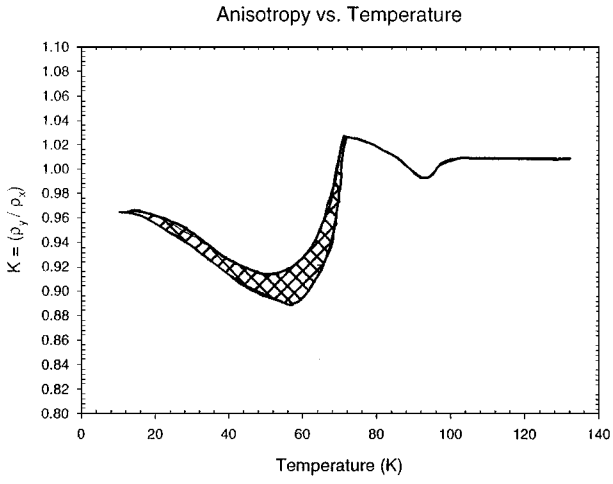

Figure 4b Plots of K versus temperature show no significant deviations from unity in the paraconductive region when an applied magnetic field causes grain-boundary dominance. However, there is a significant deviation corresponding to the width of the superconducting transition region and another deviation closer to absolute zero. The second deviation is not repeatable but over 100 test runs fell within the cross-hatched region shown.

but only on a relative basis. As shown in Fig. 4a for sample BR8, the stronger the test current the stronger the deviation in K. However, when we compared this deviation in K to other samples formed at the same stamping pressure, the deviations were markedly different. Although BR8 reached a maximum deviation of 38% at 95 mA, maximum deviations for identical samples were as low as 10% or as high as 60%.

To better understand the results in Fig. 4a, we need to consider what happens when a magnetic field is applied. As shown in Fig. 4b, the deviations of K in the paraconductivity region disappear. The paraconductivity measurements shown in Fig. 3 are due only to effects within each grain. They are not grain-boundary dependent. By contrast, the modified van der Pauw parameter K is grain-boundary dependent. In Fig. 4b, the magnetic field increases the effect of the grain boundaries. This widens the transition region as the grain boundaries take on the characteristics of the "stretched" exponential. The dominance of the grain boundaries causes the anisotropy of each grain to be hidden by the conduction processes in the sample as a whole. We can also see the effects of grain boundaries in Fig. 4a. when no magnetic field is applied but when the test current is low (5 mA). There is a threshold voltage at each grain boundary that charge carriers must have in order to tunnel between grains. At low current, the voltage drop within each grain would be much smaller than the threshold voltage at each grain boundary. Hence, the effects of the grain boundaries at low current would be to make the sample have an isotropic conduction and K would remain approximately unity throughout the temperature range of paraconductivity.

If our samples were single-crystal, deviations in K would measure anisotropy in the xy-plane. Because it is possible for each grain in a polycrystal to have an orientation different than any other grain, it is possible for K never to deviate from unity: 2-dimensional conduction in one grain might favor conduction in the x-direction while the same 2-dimensional conduction process in another grain would compensate for this by favoring y-direction conduction, and this would happen in all grains such that the average conduction was isotropic. Therefore, the fact that K does deviate from unity in certain cases for every sample we tested indicates that there are "statistically" preferred orientation angles for the sample as a whole. In Fig. 4b, the application of a magnetic field erases the effect of these "preferred" orientations in the paraconductivity region when the grain boundary effects dominate. However, the application of the magnetic field exposes two new states in the superconducting region. In the first case, there is marked anisotropy for $70 < T < T_c = 91\ K$, the width of the transition region. With no magnetic field, the width of the transition region was almost zero. The magnetic field not only widens the transition in the superconducting state, but it also marks its presence by the deviation of K from unity. This phenomenon occurs not just for BR8 but for our other samples, as well. The second state is more confusing. Our values of K for $70 > T > 0\ K$ deviated from unity each time we ran a measurement in this temperature range. However, these measurements were not repeatable. They did, however, fall into a range that we show by cross-hatched lines in Fig. 4b. This state is stable enough to have limits placed on K, but it is unstable enough to be non-repeatable from one test to the next. Data represented by the cross-hatch lines are the result of 100 test runs at many different test currents with the various currents being changed or held fixed from one run to another.

3. Conclusion

Our investigation of 2- and 3-dimensional conduction in the YBCO superconductor has confirmed the usefulness of the paraconductivity in identifying the temperature ranges over which copper planes and chains conduct. Furthermore, this is an intra-grain phenomenon,

and it is not changed by the application of an external magnetic field. Application of a magnetic field does increase the width of the temperature range over which each sample becomes fully superconducting, and the resistivity in this transition region fits a "stretched" exponential model very well. This provides us with information about the critical current and pinning potential and allows another technique for the study of grain boundary effects.

Using the van der Pauw technique to measure the resistivity and the anisotropy in resistivity, we had another tool to study dimensional conduction in our polycrystalline samples. The anisotropy, measured in this way, is affected by the sample as a whole, including the grain boundaries. If the orientation of each grain relative to all other grains were random, the "average" anisotropy for the whole sample would disappear. Our results show that there is some non-randomness in all samples, which produces a net anisotropy for the sample taken as a whole. This anisotropy is pronounced in the paraconductive temperature range, except at low test currents and/or high magnetic field strengths, where grain-boundary tunneling tends to create an average isotropy in the sample.

The van der Pauw technique of studying anisotropy is not as sharp as the study of the paraconductivity, when studying the paraconductive temperature range. However, it does complement the study of sample paraconductivity, and it is useful in studying anisotropy in the deep superconducting state ($T < T_c$). In deep superconductivity and with no magnetic field applied, the sample appears isotropic. In deep superconductivity and with an applied magnetic field, two states are visible in the appearance of strong anisotropy. The first state corresponds to the temperature range below T_c over which the sample becomes fully superconducting. (With no magnetic field applied, this temperature range is approximately zero.) The second state is chaotic and is located closer to absolute zero. Evidence of this state vanishes when there is no magnetic field applied.

In addition to our study of dimensional conduction, we found a correlation between sample porosity and resistive parameters that supports earlier theories.

4. Appendix

If a sample is in the form of a disc whose thickness is uniform but small compared to the dimensions of the sample face, then van der Pauw's theory can be used to measure the sample's resistivity [16]. The sample can have an arbitrary shape on its face (xy-plane), but it must have a constant thickness (z-axis). With four contacts placed clockwise around the perimeter, the resistivity can be calculated from voltage and current readings as

$$0 = \exp[-(\rho/d)(V_{12}/I_{34})] + \exp[-(\rho/d)(V_{23}/I_{41})] - 1 \qquad (10)$$

where d is the sample thickness and where all voltage-to-current ratios (VTCRs) are positive. V_{12} is measured across contacts 1, 2 while current I_{34} enters contact 3 and leaves at contact 4, etc. Because our data were collected by computer, we measured all eight sets of permutations of the data shown in Equation 10. For example, we used (10) with V_{23}, V_{34}, I_{41}, I_{12} and then with V_{34}, V_{41}, I_{12}, I_{23}, and then with V_{41}, I_{12}, I_{23}, I_{34}. We also reversed the polarities of the voltages and currents and measured these. This gave eight readings for the resistivity. In addition, multiple readings of each set of measurements were taken (typically 20, but as high as 100). Using 20, the average resistivity at one single temperature was the average of 160 (i.e., 8×20) measurements. The standard deviation of resistivity data was also calculated and found to be less than 0.1%. We solved Equation 10 to find resistivity by a simple "brute force" method. We assumed resistivity to be 0.000,001 and calculated the right-hand side (RHS) of Equation 10. We then let it be 0.000,002 and recalculated the RHS. We continued in this fashion until the RHS had passed zero.

Because our samples were square, the geometry allowed us to extend van der Pauw's theory to measure $K = (\rho_y/\rho_x)$ [19, 20]. This theory is an extension of the concept of image charges in electromagnetic theory, but in this case, image currents are used. With the sample in the xy-plane and with corners at (0, 0), (0, w), (w, 0) and (w, w) (w is the sample width), current, I, enters at (0, 0) and leaves at (0, w). Solving this is the same as solving for a sample of the same material but which is an infinite sheet, with current $4I$ entering the sample at (0, 0) and leaving $(-4I)$ at (0, w) and with image currents of $4I$ at the points ($2mw$, $2nw$) and currents of $-4I$) at ($(2m+1)\,w$, $2nw$), where m and n are integers ranging from negative to positive infinity. Using superposition to find the net voltage of all of these image currents yields

$$0 = (\pi d/8\rho)(V_{12}/I_{34}) + \sum_{j=0}^{j=\infty} \ln(\tanh(\pi(j+0.5)K)) \qquad (11)$$

In Equation 11 and later in 12, all VTCRs are positive. Using Equation 11, K can be solved with excellent accuracy by truncating the series at $j = 20$. A "brute force" solution, though slow, is both accurate and manageable. We start by letting $K = 20.000$ and then solve the RHS in Equation 11. We repeat for $K = 19.999$, 19.998, etc. When the RHS crosses zero, the value of K is known with an error of less than 0.001. If more accuracy is desired, the process may be extended to the fourth decimal place.

One now uses the method of image currents as above but letting the current, $4I$, enter at (0, 0) and leave at (w, 0). Then the equation to solve becomes

$$0 = (\pi d/8\rho)(V_{23}/I_{41}) + \sum_{j=0}^{j=\infty} \ln(\tanh(\pi(j+0.5)/K)) \qquad (12)$$

The solution of Equation 12 will give another value of K. Also, Equations 11 and 12 can be solved again using the VTCRs of V_{34}/I_{12} and V_{41}/I_{23}. Furthermore, all of these calculations can be done for a reversal of the polarity of the currents and voltages. This will give the eight values of K. If 20 sets of measurements are

taken, the average value of K and a standard deviation are based on 160 measurements. Standard deviations for K were less than 0.4%.

Acknowledgement

We wish to thank Prof. Leona Pisani for helpful advice in the preparation of this manuscript.

References

1. P. W. ANDERSON and Z. ZOU, *Phys. Rev. Lett.* **60** (1988) 132.
2. P. B. LITTLEWOOD and C. M. VARMA, *Phys. Rev. B* **45** (1992) 12636.
3. D. H. LIEBENBERG, R. J. SOULEN, T. L. FRANCAVILLA, W. W. FULLER-MORA, P. C. MCINTYRE and M. J. CIMA, *ibid.* **51** (1995) 11838.
4. M. S. RAVEN and Y. M. WAN, *ibid.* **51** (1995) 561.
5. S. N. BHATIA and C. P. DHARD, *ibid.* **49** (1994) 12206.
6. R. GAGNON, C. LUPIEN and L. TAILLEFER, *ibid.* **50** (1994) 3458.
7. K. TAKENAKA, K. MIZUHASHI, H. TAKAGI and S. UCHIDA, *ibid.* **50** (1994) 6534.
8. R. K. SINGH, S. D. HARKNESS, P. TIWARI, J. NARAYAN, C. JAHNCKE and M. PAESLER, *ibid.* **51** (1995) 9155.
9. W. HOLM, Y. ELTSEV and O. RAPP, *ibid.* **51** (1995) 11992.
10. Y. F. YAN, P. MATL, J. M. HARRIS and N. P. ONG, *ibid.* **52** (1995) R751.
11. P. NYHUS, M. A. KARLOW, S. L. COOPER, B. W. VEAL and A. P. PAULIKAS, *ibid.* **50** (1994) 13898.
12. W. LANG, G. HEINE, P. SCHWAB, X. Z. WANG and D. BAUERLE, *ibid.* **49** (1994) 4209.
13. L. HOU, J. DEAK, P. METCALF and M. MCELFRESH, *ibid.* **50** (1994) 7226.
14. A. GAUZZI and D. PAVUNA, *ibid.* **51** (1995) 15420.
15. R. COMBESCOT and X. LEYRONAS, *ibid.* **54** (1996) 4320.
16. L. J. VAN DER PAUW, *Phillips Res. Rep.* **13** (1958) 1.
17. H. C. MONTGOMERY, *J. App. Phys.* **42** (1971) 2971.
18. B. F. LOGAN, S. O. RICE and R. F. WICK, *ibid.* **42** (1971) 2975.
19. W. L. V. PRICE, *Sol. St. Electron.* **16** (1973) 753.
20. M. KINSLER, L. V. HMURCIK, and J. PATTON, *J. Mat. Sci.* **23** (1988) 1425.
21. L. V. HMURCIK, B. IBARRA and A. BIDARIAN, *Bull. Am. Phys. Soc.* **39** (1996) 640.
22. P. FOURNIER, M. AUBIN and M. A. R. LEBLANC, *Phys. Rev. B* **50** (1994) 9548.
23. S. A. HOFFMAN, M. A. CASTRO, G. C. FOLLIS and S. M. DURBIN, *Physica C* **59** (1993) 208.
24. M. A. CASTRO, S. M. DURBIN and M. MCELFRESH, *Phys. Rev.* B **50** (1994) 13744.
25. N. MCN. ALFORD, W. J. CLEGG, M. A. HARMER, J. D. BIRCHALL, K. KENDALL and D. H. JONES, *Nature* **332** (1988) 58.
26. J. W. EKIN, A. I. BRAGINSKI, A. J. PANSON, M. A. JANOCKO, D. W. CAPONE, N. J. ZALUZEC, B. FLANDERMEYER, O. F. DELIMA, M. HONG, J. KWO and S. H. LIOU, *J. App. Phys.* **62** (1987) 4821.
27. H. HOJAJI, K. A. MICHAEL, A. BARKATT, A. THORPE, M. WARE, I. TALMY, D. HAUGHT and S. ALTERESCU, *J. Mater. Res.* **4** (1989) 28.
28. S. JIN, T. H. TIEFEL, R. C. SHERWOOD, M. E. DAVIS, R. B. VAN DOVER, G. W. KAMMLOTT, R. A. FASTNACHT and H. D. KEITH, *App. Phys. Lett.* **52** (1988) 2074.
29. R. PETRITZ, *Phys. Rev.* **104** (1956) 1508.
30. J. CRANK, "The Mathematics of Diffusion" (Clarendon, Oxford 1956); and J. N. ROBERTS and L. M. SCHWARTZ, *Phys. Rev. B* **31** (1985) 5990.
31. KAZUO KADOWAKI, S. L. YUAN, K. KISHIO, T. KIMURA and K. KITAZAWA, *Phys. Rev. B* **50** (1994) 7230.

Received 16 September 1997
and accepted 6 August 1998